

Turbulent pipe flow at $Re_\tau \approx 1000$: A comparison of wall-resolved large-eddy simulation, direct numerical simulation and hot-wire experiment



C. Chin^{a,*}, H.C.H. Ng^a, H.M. Blackburn^b, J.P. Monty^a, A. Ooi^a

^a Department of Mechanical Engineering, University of Melbourne, Parkville, Victoria 3010, Australia

^b Department of Mechanical and Aerospace Engineering, Monash University, Clayton, Victoria 3800, Australia

ARTICLE INFO

Article history:

Received 4 November 2014

Revised 26 June 2015

Accepted 20 August 2015

Available online 31 August 2015

Keywords:

Turbulence

Wall-bounded flows

Direct numerical simulation

Wall-resolved large eddy simulation

Hot-wire experiment

ABSTRACT

Results are reported for wall-resolved large-eddy simulation of fully developed turbulent pipe flow with computational domain length $8\pi\delta$, performed using a spectral vanishing viscosity approach. Turbulence statistics are compared with direct numerical simulation and hot-wire experimental data at matched friction Reynolds number $Re_\tau = 1002$. Turbulence statistics of streamwise velocity show good agreement up to the fourth order. Analysis of the results from the transverse velocities and pressure components are also performed and found to compare well with direct numerical simulation data. The results highlight the feasibility of using wall-resolved large-eddy simulation to accurately investigate turbulent pipe flow at Reynolds numbers not currently feasible for direct numerical simulation.

© 2015 Elsevier Ltd. All rights reserved.

1. Introduction

The need to investigate fundamental wall-bounded turbulence at high Reynolds number is widely agreed in open literature. In the present age, accurate high Reynolds number data are still primarily achievable only via well designed experimental methods. With the progress of computational technology, simulations have emerged to play a vital role in the research of wall-bounded turbulence. One of the most cited articles for direct numerical simulation (DNS) of turbulent pipe flow is by Eggels et al. [13], whose dataset is commonly used to compare with experimental results. The Reynolds number in their simulations was $Re_\tau \approx 180$ ($Re_\tau = U_\tau\delta/\nu$, where friction velocity is U_τ , kinematic viscosity is ν and pipe radius is δ). Eggels et al. [13] compared DNS results with experimental results of hot-wire anemometry (HWA), particle image velocimetry (PIV) and laser Doppler anemometry (LDA) at nominally similar Reynolds number. The effects of low Reynolds number is already well documented (see [2,12,34,42]), which clearly show the maxima of the streamwise turbulence intensity and Reynolds shear stress increasing with Reynolds number. In addition, turbulence statistics that are scaled with inner variables are dependent on Reynolds number. Low Reynolds number has significant effect on the logarithm law of the mean velocity profile, which results in a greater additive constant. This is mainly due

to a higher pressure gradient effect from low Reynolds number [34]. Therefore there is a need for higher Reynolds number DNS. In recent times, there have been moderate Reynolds number DNS of turbulent pipe flows performed by [9,10,24,26,43] with Reynolds number ranging from $Re_\tau \approx 500$ to 2000. These Reynolds numbers are considered modest compared to turbulent pipe flow experiments carried out by [16,32,33,46], with a Reynolds number range of $Re_\tau \approx O(10^3 - 10^5)$.

Large-eddy simulations (LES) can provide an alternative to DNS owing to reduced computational requirements. In comparison to DNS, however, LES has not been as well received as an accurate tool for fundamental wall-bounded turbulence research, which is predominantly due to uncertainties introduced by the sub-grid-scale modelling it requires, especially in the near-wall region. There have been on-going efforts in the formulation of more accurate LES models, but comparatively few simulations have been performed at high Reynolds numbers.

To the authors' knowledge the highest Reynolds number LES of turbulent pipe flows carried out is at $Re_\tau \approx 2200$ by Berrouk et al. [4]. Their LES had wall-normal grid resolutions of two grid points within the viscous sublayer, with the first grid point at 1.3 wall units from the wall. This suggests marginal resolution to be considered a wall-resolved LES according, e.g., to the recommendations of [37], where the first grid point should be less than one wall unit away from the wall. This study is motivated by the work of [38] who performed a wall-resolved LES of a spatially evolving turbulent boundary layer, whereby the near-wall region is fully resolved.

* Corresponding author. Tel.: +61 3 83443044; Fax: +61 3 8344 4290.
E-mail address: chincc@unimelb.edu.au (C. Chin).

The aim of the present work is to carry out wall-resolved LES and to compare outcomes to those obtained by DNS and HWA at matched Reynolds number for internal wall-bounded turbulent flows. In this work, by wall-resolved LES, the authors mean an LES with DNS-like wall-normal resolution, rather than simply the LES without the wall model, which often have coarser wall-normal resolution than in the DNS. The definition is consistent with the terminology adopted by [38]. By demonstrating the accuracy of turbulence statistics we hope to advocate for the future use of wall-resolved LES for the simulation of high Reynolds number wall-bounded turbulent flows. The LES has grid points of approximately 40×10^6 as compared to the DNS with grid points of 590×10^6 . This corresponds to computational saving of the order $O(10)$.

Our LES methodology employs the ‘spectral vanishing viscosity’ (SVV) approach [20,23,29,35,41,44] in which no explicit sub-grid scale model is included, but where viscosity is increased at progressively higher wavenumbers in a numerical discretisation with underlying spectral/exponential spatial convergence properties in such a way that the outcomes smoothly approach spectral DNS as the mesh is refined. Since there is no explicit turbulence model, the method is allied to the ‘monotonically integrated’ LES (MILES) approach outlined by Fureby and Grinstein [14,15]. SVV has previously shown promising outcomes when applied to turbulent pipe flow at $Re_\tau = 314$ by Koal et al. [25]. That work employed spectral element–Fourier discretisations in which the periodic direction was azimuthal and spectral elements were used to discretise the meridional semi-plane, while in the present study we have used spectral elements to discretise the pipe cross-section and employed Fourier expansions in the axial direction.

In the work described below, we compare SVV-based LES of turbulent pipe flow at $Re_\tau = 1002$ (corresponding to Reynolds number based on bulk flow speed and pipe diameter of $Re_D = 37600$) with matching DNS and HWA measurements.

2. Numerical method

The streamwise, radial and azimuthal directions are denoted as x , r and θ , here we define $y = R - r$, where R is the pipe radius. The respective velocities are defined as U , U_r and U_θ with the corresponding fluctuating components as u , u_r and u_θ . The computational streamwise domain length is $L_x = 8\pi R$. This is based on the recommendation of [10] that turbulence statistics (up to second order) require this minimum streamwise domain length to achieve convergence at $Re_\tau = 1000$. The DNS data used in this study are from [6].

The DNS was performed using a parallel spectral element/Fourier code [5], while the LES was performed with a modified version of the same code that includes SVV, as outlined (albeit for a cylindrical coordinate implementation) by Koal et al. [25].

For both DNS and LES, the spatial discretization is fully spectral with Fourier expansions in the axial direction and with nodal-based spectral elements covering the pipe cross-section (see Fig. 1). The time-integration scheme is a second-order velocity-correction projection scheme [17,21].

The number of grid points for DNS was $N_x = 3200$, $N_r \approx 192$ and $N_\theta = 960$ in x , r and θ directions. These yield grid resolutions of $\Delta x^+ = 7.87$, $\Delta y^+ = 0.03$ at the wall and $\Delta y^+ = 8.2$ at the pipe axis and maximum $\Delta r\theta^+ = 6.56$ at the wall. (The superscript ‘+’ denotes parameters non-dimensionalised with respect to U_τ and ν .)

According to the recommendations of [37], a grid resolution sufficient for LES would be $\Delta r\theta^+ \approx 15\text{--}40$ and $\Delta x^+ \approx 50\text{--}150$. Here, the LES typically has an axial grid resolution of $\Delta x^+ = 32.8$ and maximum $\Delta r\theta^+ = 19.7$, which is within or finer than the recommended grid resolutions. To perform a wall-resolved LES, the radial grid resolution has to be fine enough to represent the structures, hence the chosen number of grid points utilized in the radial direction is $N_r \approx 160$, yielding a first grid point off the wall at $\Delta y^+ = 0.048$. There

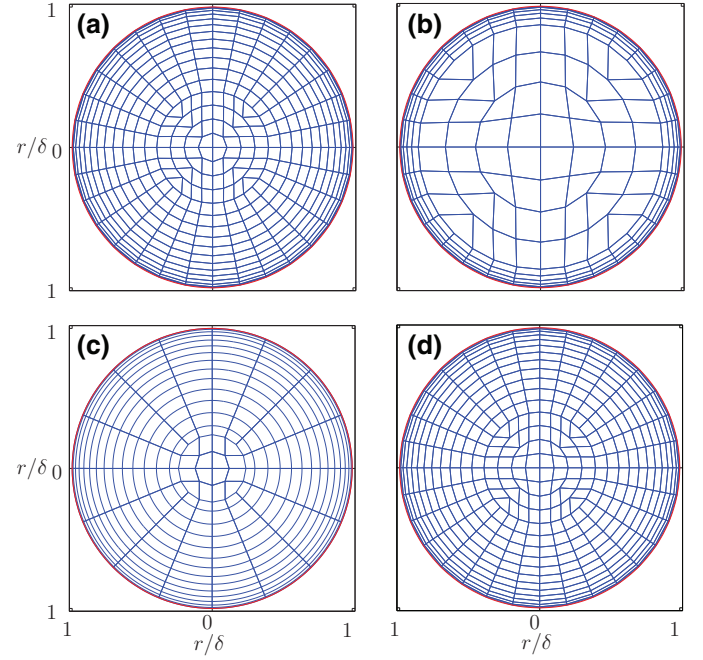


Fig. 1. Spectral elements for different simulations stated in Table 1. (a) LES1 (LES-NM uses the same grid as LES1), (b) LES2, (c) LES3 and (d) LES4.

are at least 25 grid points within the buffer layer $y^+ \approx 30$. At least five wash-through timescales (L_x/U_b) had elapsed prior to collection of turbulence statistics in order that statistically steady states were first attained. The statistics from the simulations presented here were subsequently averaged over 12 wash-through times.

SVV methodology is comparatively straightforward to understand and to implement. As outlined above, it amounts to a smoothly-varying increased viscosity as with increasing wavenumber. In the Fourier (here, the axial) direction, one implements a Fourier-mode-dependent viscosity coefficient of the form

$$\nu_k = \nu \left(1 + \frac{\epsilon}{\nu} Q_k \right), \quad (1)$$

where ν represents (kinematic) viscosity, k is an integer Fourier mode index, ϵ is a moderately small multiple of ν and Q_k is a smooth real shape function. As in the work of [28] and many subsequent authors, we use a shape function of the form

$$Q_k = \exp \left(- \frac{(N-k)^2}{(M-k)^2} \right), \quad M < k \leq N \quad (2)$$

where N is the highest Fourier mode index for the computation (if there are N_x axial data planes, $N \equiv N_x/2$). Quadrilateral nodal spectral elements are used to discretise the pipe cross-section, in which the shape functions are (isoparametrically mapped) two-dimensional tensor products of one-dimensional Lagrange interpolants through the Gauss–Lobatto–Legendre (GLL) quadrature points. In this case the derivative operator matrices used to construct diffusion operators are modified via (i) transformation to Legendre polynomial space; (ii) factorization with a diagonal matrix of form

$$\text{diag} \left(1 + \frac{\epsilon}{\nu} Q_k \right)^{1/2}, \quad (3)$$

where Q_k is of the same form as (2) but where now N is the order of the GLL Lagrange interpolants ($N = 10$ in the present work) and k is a Legendre polynomial index; and finally (iii) inverse transformation from Legendre polynomial to physical space. Refer to [25] for further details. For all the results reported here, $\epsilon = 5\nu$. For the (Fourier) pipe-axial direction, $M = 24$, while for the 10th-order spectral elements used to discretize the pipe cross-section, $M = 5$.

Table 1
Grid parameters for different LES simulations.

Simulation	Δx^+	Δy^+	$\Delta r\theta^+$	N_x	N_r	N_θ	$\frac{TU_b}{L_x}$	N_p (10^6)
LES1 (red \square)	32.8	[0.048,9.84]	19.6	768	160	320	12	35
LES2 (blue \otimes)	32.8	[0.048,23.5]	19.6	768	80	320	12	17
LES3 (grey \diamond)	32.8	[0.048,9.84]	39.3	768	160	160	12	18
LES4 (black \triangle)	65.6	[0.048,9.84]	19.6	384	160	320	12	17
LES-NM (green \boxplus)	32.8	[0.048,9.84]	19.6	768	160	320	12	35

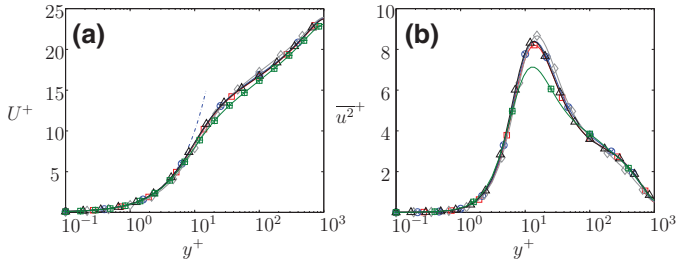


Fig. 2. Comparison of turbulent pipe flow (a) mean velocity profile and (b) streamwise turbulence intensity profile for different LES simulations as stated in Table 1. Line shown are for LES1 (red \square); LES2 (blue \otimes); LES3 (grey \diamond); LES4 (black \triangle) and LES-NM (green \boxplus). The blue dot-dashed line is $U^+ = y^+$. (For interpretation of the references to color in this figure legend, the reader is referred to the web version of this article.)

3. LES mesh resolution study

A mesh resolution study is performed beforehand to determine how the mesh resolutions in the axial, azimuthal and radial directions affect the turbulence statistics. Within each spectral element, a 10th order GLL mesh is employed.

The wall-resolved LES spectral element grid as described in Section 2 is shown in Fig. 1(a), we denote this simulation as LES1. Fig. 1(b) shows the next LES mesh (labeled as LES2) that has the same wall-normal resolution as LES1 up to $y^+ = 30$, after which, the mesh grading is coarsened to the pipe center, which corresponds to a coarser grid resolution within the element. In Fig. 1(c), the wall-normal number of elements is similar to that of LES1, while the number of elements in the azimuthal direction is reduced by half of LES1, this simulation is denoted as LES3. Fig. 1(d) presents the LES mesh for investigating the axial resolution effects, which we termed as LES4. The mesh in the wall-normal and azimuthal directions is exactly the same as LES1, the only difference is the axial resolutions is twice as coarse as that of LES1. For comparison, we have also performed an LES without SVV on the exact spectral element grid as LES1 with identical 10th order GLL mesh within each element, which is denoted as LES-NM. We have not performed LES without SVV on other cases (i.e., LES2-4) because results from LES-NM are inaccurate as will be shown later, hence it is deemed unnecessary to carry out simulations without SVV on the other coarser meshes. A summary of the different grid parameters is shown in Table 1.

Firstly the mean velocity and streamwise turbulence intensity profiles are presented in Fig. 2. The results from the LES simulations seem to collapse well with the exception of LES3 (grey \diamond) and LES-NM (green \boxplus). The mean velocity profile for LES-NM is clearly lower than the other simulations and the peak turbulence intensity is underestimated. The LES-NM can be viewed as a *coarse* DNS, since the SVV is not active. Therefore, the reason for the lower peak in the turbulence intensity is due to the coarser azimuthal grid resolution ($\Delta r\theta^+ = 19.7$, compared to DNS at $\Delta r\theta^+ = 6.56$). A coarse azimuthal grid resolution is similar to having insufficient spatial resolution and the effects have been reported by researchers such as [7,19,39,40]. One prominent effect is the decrease in peak value of turbulence intensity, which is clearly shown in Fig. 2(b). The results from LES3 over-

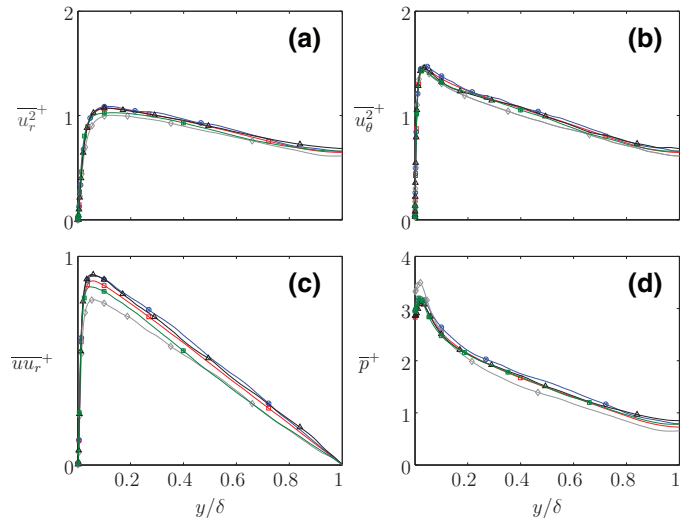


Fig. 3. Comparison of different LES cases for (a) radial turbulence intensity $\overline{u_r^2}^+$, (b) azimuthal turbulence intensity $\overline{u_\theta^2}^+$, (c) Reynolds stress $\overline{uu_r}^+$ and (d) pressure turbulence intensity \overline{p}^+ . Line symbols are as in Fig. 2. (For interpretation of the references to color in this figure legend, the reader is referred to the web version of this article.)

estimate the peak turbulence intensity value and underestimate the turbulence intensity in the outer region.

Fig. 3 displays the comparison of radial turbulence intensity, azimuthal turbulence intensity, Reynolds stress and pressure turbulence intensity. The results from all simulations for the radial and azimuthal turbulence intensities agree well. In the Reynolds stress and pressure turbulence intensity plots, LES3 clearly under predicts the Reynolds stress in the near-wall region (Fig. 3c) and over predicts the peak pressure turbulence intensity (Fig. 3d).

Next we compare the one-dimensional premultiplied energy spectra for the streamwise fluctuating velocity u in the streamwise ($\Phi_{uu,st}^+$) and spanwise ($\Phi_{uu,sp}^+$) directions as shown in Fig. 4. The results for LES2, LES3, LES4 and LES-NM are compared against LES-1 as the baseline case. The energy spectra presents the energy contribution of structures for corresponding wavelengths at a given wall-normal distance. The energy spectra are shown as contour plots as function of wall-normal location y^+ and streamwise and spanwise wavelengths (λ_x^+ and $\lambda_{r\theta}^+$ respectively). It is widely shown that the peak premultiplied streamwise energy occurs at a wall-normal location of $y^+ \approx 15$ and at wavelength of $\lambda_x^+ \approx 1000$ [10,18,32].

Here the results in Fig. 4(a), (e), and (g) show that LES1, LES2, LES4 and LES-NM produce the peak energy spectra at the correct location. LES3 (Fig. 4c) shows the peak energy slightly shifted to a location of $y^+ \approx 20$ and $\lambda_x^+ \approx 1500$. The LES4 (Fig. 4e) even though correctly predicting the peak energy location, fails to capture the small-scale energy for $\lambda_x^+ < 200$. This is clearly due to the coarse axial grid resolution employed in LES4 ($\Delta x^+ = 65.6$). In the spanwise spectra, [1,6] have shown an inner peak at $y^+ \approx 15$, $\lambda_{r\theta}^+ \approx 120$ and an outer peak at $y^+ \approx 200$, $\lambda_{r\theta}^+ \approx 0.9\delta^+$. LES1, LES2 and LES4 (Fig. 4b and f, respectively) produce the correct results for the inner and outer peaks, whereas LES3 and LES-NM (Fig. 4d and h, respectively) did not show

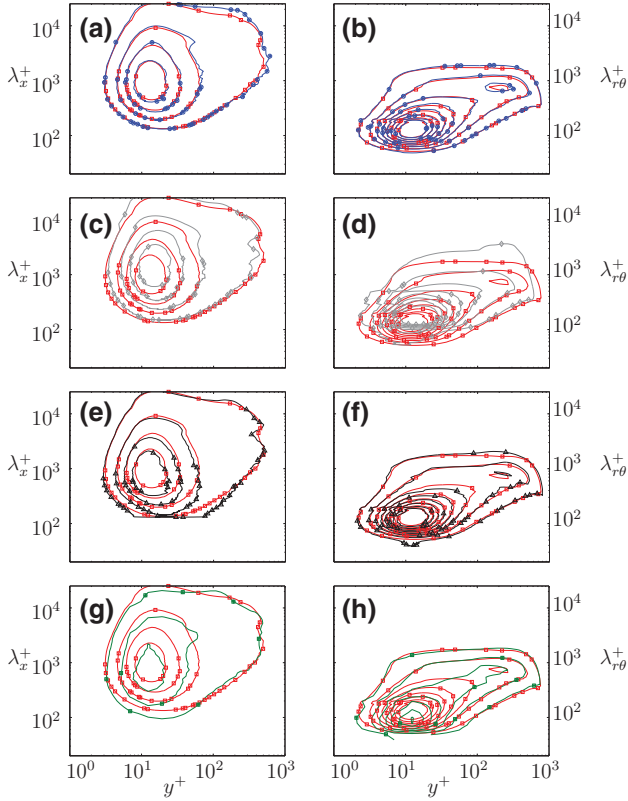


Fig. 4. Comparison of the one dimensional streamwise pre-multiplied spectra $\Phi_{uu}^+|_{sr} = k_x \phi_{uu}^+$ of u against baseline case LES-1 for (a) LES2, (c) LES3, (e) LES4 and (g) LES-NM, where k_x is the streamwise wavenumber. Comparison of the one dimensional spanwise energy spectra $\Phi_{uu}^+|_{sp} = k_y \phi_{uu}^+$ of u against baseline case LES-1 for (b) LES2, (d) LES3, (f) LES4 and (h) LES-NM, where k_y is the spanwise wavenumber. Contour levels of Φ_{uu}^+ start from 0.5 with increments of 0.5. Line symbols are as in Fig. 2. (For interpretation of the references to color in this figure legend, the reader is referred to the web version of this article.)

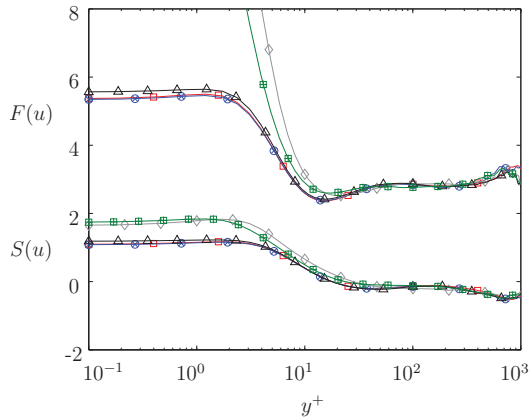


Fig. 5. Profiles of skewness (lower) and kurtosis (upper) for the different LES simulations. Line symbols are as in Fig. 2. (For interpretation of the references to color in this figure legend, the reader is referred to the web version of this article.)

the existence of an outer peak. LES3 predicts the inner peak at a greater spanwise wavelength $\lambda_{r\theta} \approx 200$ and LES-NM underestimated the inner peak at $\lambda_{r\theta} \approx 80$.

Lastly, we present the skewness and kurtosis profiles in Fig. 5. The skewness profiles are shown by the lower profiles and kurtosis profiles are the upper profiles. Once again, LES3 and LES-NM show significant discrepancies from the other LES results. Collectively, the results presented in this section can be summarised showing how different grid resolutions affect turbulence statistics and this is shown

in Table 2. The turbulence statistics have been compared with DNS results to assess the accuracy. If the compared turbulence statistic is within 5% error of the DNS, we would consider it as being accurate. A tick (✓) symbol corresponds to the LES grid being able to produce the associated turbulence statistics accurately and a cross (×) symbol indicates that the LES grid does not yield an accurate result.

From Table 2, the findings show that LES1 and LES2 produces similar results. This suggests that an LES (LES2) with a well resolved wall-normal resolution (to $y^+ \approx 30$, after which, wall-normal resolution can be relaxed) produces comparable results to an LES (LES1) with finer wall-normal resolution (above $y^+ \approx 30$). In this study, we did not perform a resolution study into the upper limit of the wall-normal resolution before results differ. No doubt with a coarser mesh, which corresponds to lower computational cost, would make LES an even more attractive alternative to simulate high Reynolds number flows. From this section onward, we have arbitrarily chosen LES1 for performing comparison with DNS and experimental results (see Table 3).

4. Experimental method

The streamwise velocity data from the simulations are compared to streamwise velocity data recorded in pipe flow where the Reynolds number ($Re_\tau \approx 1023$) was closely matched to that of the simulations, using a single-point hot-wire measurement of matched measurement spatial resolution. The experimental data employed in this paper is taken from [33]. The effect of hot-wire measurement spatial resolution for wall-bounded turbulent flows is well documented by [7,19,27] and it is understood that the turbulence intensity is attenuated at large viscous scaled wire lengths, l^+ . In a channel flow simulation, the spanwise grid spacing (defined as Δz^+) is analogous to the spatial filtering imposed by a hot-wire sensor. The sparser the spanwise spacing in viscous units (Δz^+), the greater is the severity of attenuation of the streamwise turbulence intensity [7]. In a pipe flow simulation, however, the grid is defined in cylindrical coordinates and as a result the “spanwise” grid spacing is best estimated by $\Delta(r\theta)^+$. This is maximum at the wall and approaches zero at the pipe centreline. While spatial resolution corrections for hot-wire measurements of wall-bounded turbulence have recently become available [8,30,40], we have opted to try and match measurement resolutions rather than apply a correction in post processing. In the DNS data presented here, $\Delta(r\theta)^+ = 6.56$ at the wall, which is very close to the viscous-scaled hot-wire length $l^+ = 7.6$ used in the physical HWA experiment. The HWA circuit used was a custom built Melbourne University Constant Temperature Anemometer (MUCTA II) operated with an overheat ratio of 1.8. The hot-wire sensing element was etched to a length of $l = 0.36$ mm from platinum core Wollaston wire with a core diameter of $d = 1.5$ μ m. This provided a non-dimensional wire length of $l^+ = lU_\tau/\nu = 7.6$ and a hot-wire length-to-diameter ratio of $l/d = 244$. The system frequency response to a 1 kHz square wave was set to a frequency corresponding to $t^+ \lesssim 1$ which equated to greater than 75 kHz. These measurements were conducted in the pipe flow facility at The University of Melbourne described by Perry et al. [36] and is part of a data base of pipe and channel streamwise velocity data reported in [33]. All relevant parameters pertaining to the current comparison, for the simulations (LES1 and DNS) and the hot-wire experiment, are summarised in Table 3.

5. Results

We will first analyse the mean flow turbulence statistics to ensure results are well converged. Some of the computed mean turbulence statistics are the bulk velocity

$$\pi R^2 U_{\text{bulk}} = 2\pi \int_0^R rU(r) dr, \quad (4)$$

Table 2

Summary of the effects on turbulence statistics due to different LES grid resolutions. Symbol ✓ indicates result is within 5% error of the DNS.

Grid	U^+	$\overline{u^2}^+$	$\overline{u^2}^+$	$\overline{u^2}^+$	\overline{uu}^+	\overline{p}^+	$\Phi_{uu,st}^+$	$\Phi_{uu,sp}^+$	$S(u)$	$F(u)$
LES1	✓	✓	✓	✓	✓	✓	✓	✓	✓	✓
LES2	✓	✓	✓	✓	✓	✓	✓	✓	✓	✓
LES3	✓	×	×	✓	×	×	×	×	×	×
LES4	✓	✓	✓	✓	✓	✓	×	×	✓	✓
LES-NM	×	×	×	✓	×	×	×	×	×	×

Table 3

Experimental conditions and computational parameters for both physical and numerical experiments.

Experiment	U_{cl}	Re_τ	$d(\mu\text{m})$	$l(\text{mm})$	l^+	l/d	Δt^+	$f_s(\text{kHz})$	$\frac{Tu_d}{\delta}$
HWA (○)	7.68	1023	1.5	0.366	7.6	244	0.22	30	23305
Simulation	L_x	Re_τ	Δx^+	Δy^+	$\Delta r\theta^+$	N_x	N_r	N_θ	$\frac{Tu_h}{L_x}$
DNS (▽)	$8\pi R$	1002	7.87	[0.03,8.2]	6.56	3200	192	960	12
LES1 (□)	$8\pi R$	1002	32.8	[0.048,9.84]	19.6	768	160	320	12

Table 4

Comparison of mean flow statistics from DNS, LES and HWA.

	U_{cl}/U_τ	U_{bulk}/U_τ	U_{cl}/U_{bulk}	C_f	δ^*	θ^*	$H = \delta^*/\theta^*$
DNS	23.57	18.87	1.25	0.0056	0.105	0.071	1.478
LES	23.74	19.16	1.24	0.0054	0.102	0.070	1.456
HWA	23.59	18.76	1.26	0.0057	0.092	0.067	1.382

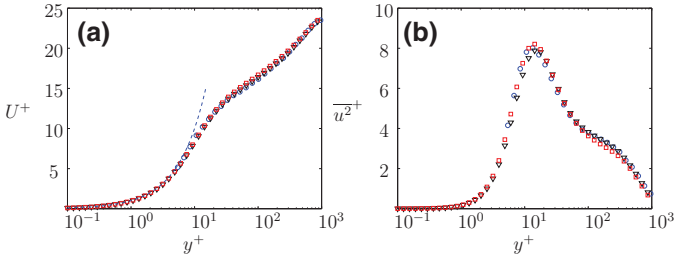


Fig. 6. Comparison of turbulent pipe flow (a) mean velocity profile in inner scaling and (b) streamwise turbulence intensity profile in inner scaling from hot-wire measurement (blue ○); DNS (black ▽) and LES (red □). Dashed line is $U^+ = y^+$. (For interpretation of the references to color in this figure legend, the reader is referred to the web version of this article.)

the displacement thickness δ^* and momentum thickness θ^*

$$\delta^*(2R - \delta^*) = 2 \int_0^R r \left(1 - \frac{U(r)}{U_{cl}}\right) dr, \quad (5)$$

and

$$\theta^*(2R - \theta^*) = 2 \int_0^R r \left(\frac{U(r)}{U_{cl}}\right) \left(1 - \frac{U(r)}{U_{cl}}\right) dr, \quad (6)$$

respectively, and the skin friction coefficient,

$$C_f = \tau_w / \frac{1}{2} \rho U_{bulk}^2, \quad (7)$$

where τ_w is the wall shear stress. A summary of the mean turbulence statistics is presented in Table 4. The LES here compares exceptionally well with the DNS, with an average error of 0.7%. When compared with the HWA data, the average error is 4.6%. This slight discrepancies between the results could be due to experimental limitations in the near-wall where measurements are not obtained. Fig. 6(a) and (b) display the mean velocity and turbulence intensity profiles, in inner scaling, for the simulations and experiment. The DNS is represented by triangle symbols, LES by squares and HWA by circles. The mean velocity profiles collapse remarkably well throughout the flow with

the simulations capturing data within the linear sublayer, which is absent from the hot-wire data due to wall proximity limitations in the experiment. The turbulence intensity profiles agree well for most of the flow and behave as expected, peaking at an inner-scaled wall normal distance of $y^+ \approx 15$. The peak values of $\overline{u^2}^+ = 7.99$ and 8.02 for the hot-wire and LES respectively are slightly higher than that of the DNS which peaks at $\overline{u^2}^+ = 7.9$, a difference of approximately 1.5%. Results here are also in good agreement with [43] who report the statistics of a turbulent pipe flow DNS conducted at $Re_\tau = 1142$. The largest discrepancy between the data from [43] and the data presented in this paper are at the pipe centerline, where we find the average non-dimensional centreline velocity to be $U_{cl}^+ \approx 23.6$, whereas Wu and Moin [43] reported a value of $U_{cl}^+ = 24.1$, a difference of approximately 2%, which is likely due to a slightly higher Reynolds number.

Having established the good agreement of mean statistics between DNS, LES and HWA, we now present and compare the one-dimensional pre-multiplied streamwise velocity spectra non-dimensionalised with friction velocity $\Phi_{uu}^+ = k_x \phi_{uu}^+$, where k_x is the streamwise wavenumber, which for the HWA data is inferred from Taylor's hypothesis using the mean velocity as the convection velocity. All energy spectra are presented as a function of the streamwise wavelength $\lambda_x^+ = 2\pi/k_x^+$. The energy spectra are presented in pre-multiplied form because, graphically, the area under the spectra is equivalent to the turbulence intensity. The spectra from the HWA time-series was computed using records of 4.5×10^6 samples, split into windows corresponding to $\lambda_x^+ = 10^5$. As k_x is estimated from the local mean velocity, the window size varied with wall distance. This upper limit was selected so that the largest wavelength equates to $\lambda_x/R \approx 100$, which should be sufficient to correctly capture the largest scale of motion. To effectively compare the energy spectra, the LES/DNS data are zero-padded to match the chosen largest wavelength. The energy spectra is spatially averaged in the azimuthal direction and temporally averaged over 80 realizations (obtained over 12 wash-through). It is more convenient to present the overall spectral energy distribution Φ_{uu}^+ as a function of both streamwise wavelength λ_x^+ and wall distance y^+ . Fig. 7 displays this global view, and reveals several aspects that were not readily apparent when viewing single point comparisons. All spectrograms compare well except in the near-wall ($y^+ < 10$) for HWA, due to limitations of the experiment as previously discussed. Hence it reinforces the need for simulations, where near-wall data can be obtained with accuracy. To further scrutinize the data, the energy spectra at selected wall normal locations of $y^+ = 15, 120, 250$ and 500 are presented in Fig. 8. Two important results can be inferred from the plots. Firstly, the energy spectra of the LES collapse surprisingly well with the DNS, except for

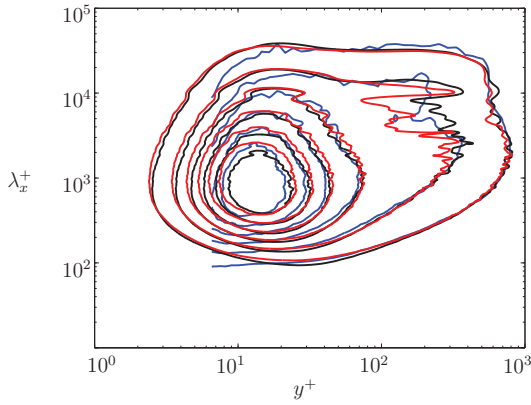


Fig. 7. Contour plot of one dimensional pre-multiplied energy spectra of streamwise velocity for HWA (blue), DNS (black) and LES (red). Contour levels of Φ_{uu}^+ start from 0.3 with increments of 0.3. (For interpretation of the references to color in this figure legend, the reader is referred to the web version of this article.)

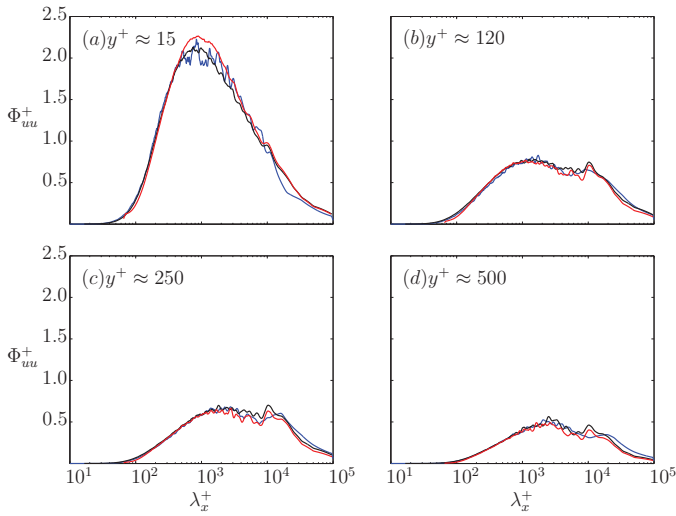


Fig. 8. Line plots of one dimensional pre-multiplied energy spectra of streamwise velocity for HWA (blue); DNS (black) and LES (red). Wall normal locations: (a) $y^+ \approx 15$, (b) $y^+ \approx 120$, (c) $y^+ \approx 250$ and (d) $y^+ \approx 500$. (For interpretation of the references to color in this figure legend, the reader is referred to the web version of this article.)

a slight over-prediction in the peak Φ_{uu}^+ value for wall-normal location $y^+ \approx 15$ (Fig. 8a). Even with a slight over-prediction in the peak value, the location of the peak coincides with the DNS at $\lambda_x^+ \approx 800$. At other wall-normal locations, the LES is able to accurately represent the entire range of length scales (restricted only by the smallest streamwise grid resolution Δx^+). In addition the LES is able to characterize the small length scales $\lambda_x^+ \leq 500$ surprisingly well (see Figs. 7 and 8). Secondly, in spite of using the local mean velocity as the convection velocity in the HWA data, good agreement with the DNS/LES is observed for the large range of scales for wall-normal locations up to $y^+ \approx 250$. There does not appear to be any small scale attenuation due to spatial filtering owing to the slightly mismatched values of l^+ and $\Delta(r\theta)^+$. Hence, emphasizing the need to compare experimental and numerical results at similar spanwise resolution. At $y^+ \gtrsim 500$ as shown in Fig. 8(d), the energy spectra still match well for a large range of scales, however, the hot-wire spectra is now clearly more energetic for wavelengths beyond $\lambda_x^+ \approx 20000$ or $\lambda_x/R \approx 20$. The differences in the spectra described here are entirely consistent with an error induced by the use of a constant convection velocity for the hot-wire time series data (for a given wall distance). del Álamo and Jiménez [11] reported for channels that the small scales convect at close to the local mean velocity, except very close to the wall, and the large

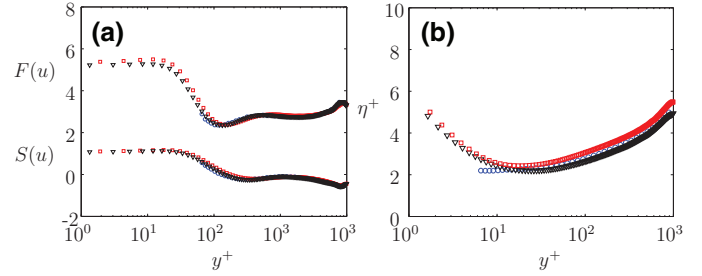


Fig. 9. (a) Profiles of skewness(lower) and kurtosis(upper). (b) Distribution of the dissipation scale in a fully developed turbulent pipe flow for $Re_\tau = 1000$. Symbols are as in Fig. 6. (For interpretation of the references to color in this figure legend, the reader is referred to the web version of this article.)

scales convect at some proportion of the bulk velocity. It should be noted that the DNS/LES spectra and the hot-wire spectra match well at wavelengths corresponding to the energy signature of the large and very-large scale motions (LSM/VLSM) first reported by Kim and Adrian [22]. This is in contrast to what [31] reported in their comparison of channel flow DNS and experiment and suggested that the scale dependency of the convection velocity differs between these internal geometries.

Fig. 9 (a) displays the skewness and kurtosis profiles of the present DNS, LES and HWA. Skewness profiles are the lower profiles and kurtosis profiles are the upper profiles, with symbols retaining their meaning from Fig. 6. All profiles agree well throughout the entire wall-normal direction with the DNS and LES being able to capture much more information very close to the wall. Once again the LES shows convergence with DNS even at high order statistics. Such excellent agreement of the higher order moments between DNS, LES and HWA, even in the far outer region, indicate that the simulations are very well converged.

Returning to spatial resolution considerations, it should be noted that a direct comparison of measurement resolutions is complicated for pipe flows by the fact that $\Delta(r\theta)^+$ decreases when moving away from the wall and is not a straightforward analogue to hot-wire length that Δz^+ is in a channel flow. Thus a more appropriate length scale to use when discussing measurement resolution may be the Kolmogorov length scale $\eta = (\nu^3 / \langle \epsilon \rangle)^{1/4}$ where $\langle \epsilon \rangle$ is the mean dissipation rate. Integration of the dissipation spectra using the method outlined by Bailey et al. [3] yielded an isotropic estimate of the mean dissipation rate $\langle \epsilon \rangle$ and the distribution of the dissipation scale η^+ is displayed in Fig. 9(b) with symbols as in Fig. 6. All distributions display a similar profile and within the region of $10 \leq y^+ \leq 50$, $\eta^+ \approx 2$ which is consistent with the results of [45] who report that η^+ is constant, independent of y^+ and Reynolds number, within the sublayer of pipe flow. At the near-wall for $y^+ \lesssim 10$, the HWA data seem to remain constant where the DNS/LES data increase rapidly as the wall is approached. As the mean dissipation rate approaches zero at the wall, one would expect η^+ to increase. The discrepancy in η^+ profiles between HWA and DNS/LES is caused by errors introduced by using the local mean velocity as the convection velocity. Since $\langle \epsilon \rangle$ for the HWA is estimated using the one-dimensional power spectra, an over-estimation of the small scales in the hot-wire spectra at $y^+ \leq 10$ (see Fig. 7) will lead to an overestimation of $\langle \epsilon \rangle$ and thus an underestimation of η^+ . It is evident from the results that wall-resolved LES at moderate Reynolds number can emulate DNS in generating accurate streamwise velocity turbulence statistics (up to fourth order).

After comparison of different u turbulence statistics for DNS, LES and HWA, it appears that HWA can be used to obtain accurate statistics, hence leading to the question why should one use wall-resolved LES. Wall-resolved LES would be practical only if turbulence statistic of the transverse velocity component can achieve accurate results as well, since accurate transverse velocities are harder to

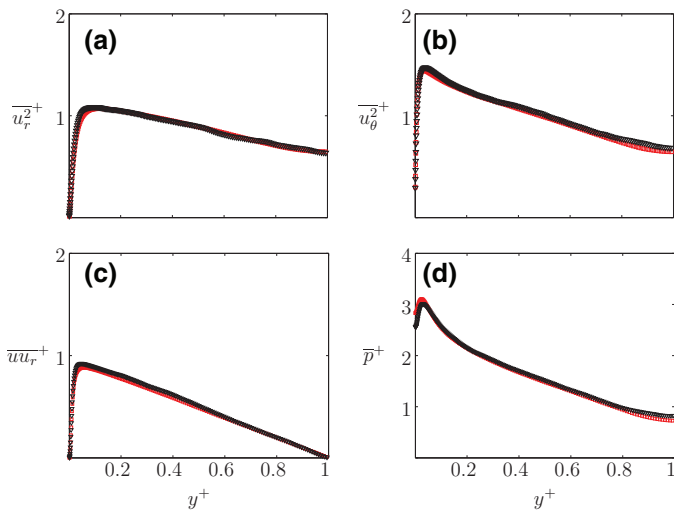


Fig. 10. Comparison between DNS (black) and LES (red) of (a) turbulence intensity u_r ; (b) turbulence intensity u_θ ; (c) Reynolds shear stress and (d) pressure fluctuation intensity. (For interpretation of the references to color in this figure legend, the reader is referred to the web version of this article.)

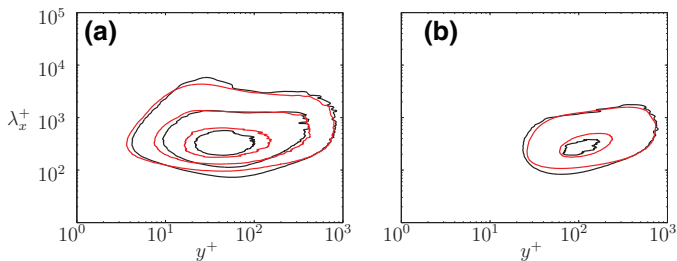


Fig. 11. Comparison of the one-dimensional pre-multiplied energy spectra between DNS (black) and LES (red) for (a) $\Phi_{u_r u_r}^+$ and (b) $\Phi_{u_\theta u_\theta}^+$. Contours begin at 0.2 with increments of 0.2. (For interpretation of the references to color in this figure legend, the reader is referred to the web version of this article.)

obtain in experiments. Fig. 10(a)–(c) show comparison of the turbulence intensities for u_r , u_θ and the Reynolds stress. There seems to be good agreement between the LES and DNS. In Fig. 10(d), the fluctuating pressure intensity is displayed. In the near-wall region, the LES tends to slightly over-predict the peak pressure fluctuation intensity by approximately 3%, but collapses with the DNS profile away from the wall. The spectrogram of the one-dimensional energy spectra for u_r and u_θ are next analysed in Fig. 11. Once again the LES displays very similar trend to the DNS for both energy spectra. Overall results seems to indicate that wall-resolved LES is suitable as a tool to simulate accurate turbulent pipe flows, at least up to the current Reynolds number.

It is shown that at high Reynolds number, it is the large-scale motions that change, while the small-scales remain invariant [19]. While it is expected that if one maintains the grid resolutions (in viscous scaling) similar to LES1 for high Reynolds number simulations, small-scales would be captured relatively well. However, it is unclear how fundamental quantities could be affected by the large-scale motions at high Reynolds number using wall-resolved LES.

6. Conclusions

In summary, a new pipe flow wall-resolved LES at $Re_\tau = 1002$ is performed. The results are compared to DNS and hot-wire data to assess the viability of the wall-resolved LES for future high Reynolds number simulations. Mean turbulence statistics for the streamwise velocity component, up to the fourth order, displayed excellent

agreement when compared with the DNS and HWA. The turbulence statistics for transverse velocities and pressure fluctuations also compare well with DNS results. There are several clear advantages of performing wall-resolved LES, one of which is that wall-resolved LES in this study used approximately 7% (≈ 40 million points) of the total grid points of the DNS (≈ 590 million points), which clearly corresponds to a substantial reduction in computational resources. In addition, it is shown that wall-resolved LES can produce accurate results comparable to HWA and DNS, furthermore, near-wall turbulence statistics are well represented, which are difficult to obtain for experiments especially at high Reynolds number. In addition, the results taken from this study in conjunction with those by Schlatter et al. [38] provide evidence that wall-resolved LES seems to produce comparable results to DNS independent of the subgrid-scale model employed, at least for high-order methods. Therefore, it is advocated that one could use any choice of subgrid-scale model when performing LES while maintaining the wall-normal resolution comparable to DNS in order to obtain accurate results.

Acknowledgments

This research was undertaken with the assistance of resources provided at the NCI NF through the National Computational Merit Allocation Scheme supported by the Australian Government. The authors also acknowledge the Victorian Life Sciences Computation Initiative for the computational resources, and the financial support of the Australian Research Council.

References

- [1] Ahn J, Lee JH, Jang SJ, Sung HJ. Direct numerical simulations of fully developed turbulent pipe flows for $Re_\tau = 180, 544$ and 934 . *Int J Heat Fluid Flow* 2013;44:222–8.
- [2] Antonia RA, Teitel M, Kim J, Browne LWB. Low-Reynolds-number effects in a full developed turbulent channel flow. *J Fluid Mech* 1992;236:579–605.
- [3] Bailey SCC, Hultmark M, Schumacher J, Yakhot V, Smits AJ. Measurement of local dissipation scales in turbulent pipe flow. *Phys Rev Lett* 2009;103(1):014502–1–4.
- [4] Berrouk AS, Laurence D, Riley JJ, Stock DE. Stochastic modelling of inertial particle dispersion by subgrid motion for LES of high Reynolds number pipe flow. *J Turb* 2007;8(50):1–20.
- [5] Blackburn HM, Sherwin SJ. Formulation of a Galerkin spectral element–Fourier method for three-dimensional incompressible flows in cylindrical geometries. *J Comput Phys* 2004;179:759–78.
- [6] Chin C. Numerical study of internal wall-bounded turbulent flows. University of Melbourne; 2011. (Ph.D. thesis).
- [7] Chin C, Hutchins N, Ooi ASH, Marusic I. Use of DNS data to investigate spatial resolution issues in measurements of wall bounded turbulence. *Meas Sci Tech* 2009;20(11):115401–1–10.
- [8] Chin C, Hutchins N, Ooi ASH, Marusic I. Spatial resolution correction for hot-wire anemometry in wall turbulence. *Exp Fluids* 2011;50:1443–53.
- [9] Chin C, Monty JP, Ooi A. Reynolds number effects in DNS of pipe flow and comparison with channels and boundary layers. *Int J Heat Fluid Flow* 2014;45:33–40.
- [10] Chin C, Ooi ASH, Marusic I, Blackburn HM. The influence of pipe length on turbulence statistics computed from direct numerical simulation data. *Phys Fluids* 2010;22(11):115107–1–10.
- [11] del Álamo J, Jiménez J. Estimation of turbulent convection velocities and corrections to Taylor's approximation. *J Fluid Mech* 2009;640:5–26.
- [12] den Toonder MJM, Nieuwstadt FTM. Reynolds number effects in a turbulent pipe flow for low to moderate Re . *Phys Fluids* 1997;9(11):3398–409.
- [13] Eggels JGM, Unger F, Weiss MH, Westerweel J, Adrian RJ, Friedrich R, et al. Fully developed turbulent pipe flow: a comparison between direct numerical simulation and experiment. *J Fluid Mech* 1994;268:175–209.
- [14] Fureby C, Grinstein FF. Monotonically integrated large eddy simulation of free shear flows. *AIAA J* 1999;37(5):544–56.
- [15] Fureby C, Grinstein FF. Large eddy simulation of high-Reynolds-number free and wall-bounded flows. *J Comput Phys* 2002;181:68–97.
- [16] Guala M, Hommema SE, Adrian RJ. Large-scale and very-large-scale motions in turbulent pipe flow. *J Fluid Mech* 2006;554:521–42.
- [17] Guermond JL, Shen J. Velocity-correction projection methods for incompressible flows. *SIAM J Numer Anal* 2003;41:112–34.
- [18] Hoyas S, Jiménez J. Scaling of velocity fluctuations in turbulent channel flows up to $Re_\tau = 2003$. *Phys Fluids* 2006;18(011702):1–4.
- [19] Hutchins N, Nickels TB, Marusic I, Chong MS. Hot-wire spatial resolution issues in wall-bounded turbulence. *J Fluid Mech* 2009;635:103–36.
- [20] Karamanos G-S, Karniadakis GE. A spectral vanishing viscosity method for large-eddy simulations. *J Comput Phys* 2000;163:22–50.
- [21] Karniadakis GE, Israeli M, Orszag SA. High-order splitting methods for the incompressible Navier–Stokes equations. *J Comput Phys* 1991;97:414–43.

- [22] Kim KC, Adrian RJ. Very large-scale motion in the outer layer. *Phys Fluids* 1999;11(2):417–22.
- [23] Kirby RM, Sherwin SJ. Stabilisation of spectral/hp element method through spectral vanishing viscosity: Application to fluid mechanics modelling. *Comp Meth Appl Mech Eng* 2006;195:3128–44.
- [24] Klewicki J, Chin C, Blackburn HM, Ooi A, Marusic I. Emergence of the four layer dynamical regime in turbulent pipe flow. *Phys Fluids* 2012;24:045107-1–14.
- [25] Koal K, Stiller J, Blackburn HM. Adapting the spectral vanishing viscosity method for large-eddy simulations in cylindrical configurations. *J Comput Phys* 2012;231:3389–405.
- [26] Lee JH, Sung HJ. Comparison of very-large-scale motions of turbulent pipe and boundary layer simulations. *Phys Fluids* 2013;25:045103-1–17.
- [27] Ligrani PM, Bradshaw P. Spatial resolution and measurement of turbulence in the viscous sublayer using subminiature hot-wire probes. *Exp Fluids* 1987;5:407–17.
- [28] Maday Y, Ould Kaber SM, Tadmor E. Legendre pseudospectral viscosity method for nonlinear conservation laws. *SIAM J Numer Anal* 1993;30:321–42.
- [29] Minguez M, Pasquetti R, Serre E. High-order large-eddy simulation of flow over the “Ahmed body” car model. *Phys Fluids* 2008;20:095101-1–17.
- [30] Monkewitz PA, Duncan RD, Nagib HM. Correcting hot-wire measurements of stream-wise turbulence intensity in boundary layers. *Phys Fluids* 2010;22(9):091701-1–4.
- [31] Monty JP, Chong MS. Turbulent channel flow: Comparison of streamwise velocity data from experiments and direct numerical simulation. *J Fluid Mech* 2009;633:461–74.
- [32] Monty JP, Stewart JA, Williams RC, Chong MS. Large-scale features in turbulent pipe and channel flows. *J Fluid Mech* 2007;589:147–56.
- [33] Ng HCH, Monty JP, Hutchins N, Chong MS, Marusic I. Comparison of turbulent channel and pipe flows with varying Reynolds number. *Exp Fluids* 2011;51:1261–81.
- [34] Nickels TB. Inner scaling for wall-bounded flows subject to large pressure gradients. *J Fluid Mech* 2004;521:217–39.
- [35] Pasquetti R. Spectral vanishing viscosity method for large-eddy simulation of turbulent flows. *J Sci Comp* 2006;27(1–3):365–75.
- [36] Perry AE, Henbest S, Chong MS. A theoretical and experimental study of wall turbulence. *J Fluid Mech* 1986;165:163–99.
- [37] Piomelli U. Large-eddy simulations: where we stand. In: Liu C, Liu Z, editors. *Advances in DNS/LES*. Columbus: Greyden Press; 1997. p. 93–104.
- [38] Schlatter P, Li Q, Brethouwer G, Johansson AV, Henningson DS. Simulations of spatially evolving turbulent boundary layers up to $Re_\theta = 4300$. *Int J Heat Fluid Flow* 2010;31:251–61.
- [39] Segalini A, Cimarelli A, Ruedi JD, de Angelis E, Talamelli A. Effect of the spatial filtering and alignment error of hot-wire probes in a wall-bounded turbulent flow. *Meas Sci Tech* 2011;22:105408-1–10.
- [40] Smits AJ, Monty J, Hultmark M, Bailey SCC, Hutchins N, Marusic I. Spatial resolution correction for wall-bounded turbulence measurements. *J Fluid Mech* 2011;676:41–53.
- [41] Tadmor E. Convergence of spectral methods for nonlinear conservation laws. *SIAM J Num Anal* 1989;26(1):30–44.
- [42] Wagner C, Hüttl TJ, Friedrich R. Low-Reynolds-number effects derived from direct numerical simulations of turbulent pipe flow. *Comput. Fluids* 2001;30:581–90.
- [43] Wu X, Moin P. A direct numerical simulation study on the mean velocity characteristics in turbulent pipe flow. *J Fluid Mech* 2008;608:81–112.
- [44] Xu C, Pasquetti R. Stabilized spectral element computations of high Reynolds number incompressible flows. *J Comput Phys* 2004;196:680–704.
- [45] Yakhot V, Bailey SCC, Smits AJ. Scaling of global properties of turbulence and skin friction in pipe and channel flows. *J Fluid Mech* 2010;652:65–73.
- [46] Zagarola MV, Smits AJ. Mean flow scaling in turbulent pipe flow. *J Fluid Mech* 1998;373:33–79.